Comparison of electromechanical transfer matrix models for passive damping involving an array of shunted piezoelectric patches

Jean-François Deü, Boris Lossouarn, Mathieu Aucejo

Florence, Italy 12-16 July 2015
ICSV22
The 22nd International Congress on Sound and Vibration

COMPARISON OF ELECTROMECHANICAL TRANSFER MATRIX MODELS FOR PASSIVE DAMPING INVOLVING AN ARRAY OF SHUNTED PIEZOELECTRIC PATCHES

Jean-François Deü, Boris Lossouarn, Mathieu Aucejo
Structural Mechanics and Coupled Systems Laboratory, Conservatoire National des Arts et Métiers, 2 rue Conté, 75003 Paris, France
email: jean-francois.deu@cnam.fr

In piezoelectric shunt damping, an array of patches can be a solution to control vibration over a broad frequency range. Implementing a multimodal electrical network gives the possibility to act on several mechanical modes simultaneously. For the study of one-dimensional structures, a periodic layout enables the use of a transfer matrix method that applies on electromechanical state-vectors. Various models can be used to describe the electromechanical unit cells. Indeed, even if the electrical medium is discrete, the mechanical structure can be approximated either by its discrete equivalent, by its homogenized forms or by its finite element model. Offering an increasing complexity, those formulations are compared in order to define their respective limits. It is especially focused on vibration reduction expectations when the considered wavelength is approaching the length of the piezoelectric patches. Depending on the frequency range of interest, it is then possible to choose a suitable model for the analysis of damping systems involving a piezoelectric network.

1. Introduction

Charge cancellation or vibration node locations induce that a single shunted piezoelectric patch cannot consistently achieve a multimodal control. In order to sense and control vibration over a prescribed frequency range, a solution consists in using an array of piezoelectric patches [1] which is small enough compared to the smallest wavelength to control. Then, as an extension of the tuned mass damping strategy, a passive multimodal control requires the implementation a network whose modes are close to those of the controlled structure [2]. This can be achieved by connecting the mechanical structure to its discrete electrical analogue through the array of piezoelectric patches [3]. When considering one-dimensional periodic structures, it becomes possible to employ a transfer matrix method that applies on state-vectors including both mechanical and electrical variables. Various models can be used to describe the electromechanical unit cells. The electrical medium remains discrete but the mechanical structure can be approximated by its discrete equivalent, by its homogenized forms, or by its finite element model. In this contribution, these transfer matrix models of increasing complexity are compared for studying the damping of longitudinal wave propagation in rods. The main objective is to define their respective limits and select the most appropriate one depending on the frequency range of interest and the required accuracy.

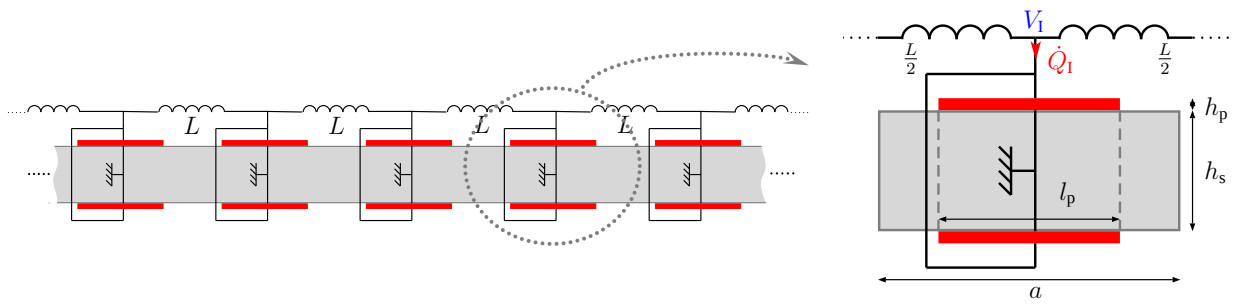

Figure 1: Networked array of piezoelectric patches and corresponding electromechanical unit cell.

2. Periodic piezoelectric array on a one-dimensional structure

2.1 Electromechanical unit cell

An array of piezoelectric patches is periodically distributed on a one-dimensional homogeneous structure. The patches are connected together through an electrical networks that is also periodic. As seen in Fig. 1, it is chosen to consider the example of a line of inductors that is connected to paralleled pairs of piezoelectric patches. As this network is the electrical analogue of a longitudinal lattice of point masses, it can lead to a broadband control of longitudinal waves [3]. As an electromechanical periodic structure is obtained, it is possible to extract the unit cell that repeats along the main direction. This unit cell of length a, and width b is represented in Fig. 1. The thicknesses of the main structure is h_s, the thickness of the patches is also h_s and their length is l_p. $\dot{Q}_I$ is the current flowing into the pair of patches and V_I is the voltage on the electrodes connected to the network. The two piezoelectric patches need to be transversely polarized in opposite directions in order to generate a non-zero voltage when longitudinal excitation occurs [1].

2.2 One-dimensional behavior of a thin piezoeletric patch

A single piezoelectric patch can be described under a plane-stress assumption by the following one-dimensional formulation, which is obtained from the 3D linear piezoelectricity theory [4]:

$$(1) \qquad \begin{cases} \sigma_p = Y_p^E \varepsilon_p - \bar{e}_{31} E_p, \\ D_p = \bar{e}_{31} \varepsilon_p + \bar{\epsilon}_{33}^{\varepsilon} E_p \end{cases} \quad \text{where} \quad Y_p^E = \frac{1}{s_{11}^E}, \quad \bar{e}_{31} = \frac{d_{31}}{s_{11}^E}, \quad \text{and} \quad \bar{\epsilon}_{33}^{\varepsilon} = \epsilon_{33}^{\sigma} - \frac{d_{31}^2}{s_{11}^E}.$$

The strain ε_p and the stress σ_p represent the mechanical behavior in the axial direction '1' and D_p and E_p are the electric displacement and electric field in the transverse direction '3'. Concerning the material constants, s_{11}^E is the elastic compliance at constant electric field, d_{31} is the piezoelectric charge constant and ϵ_{33}^{σ} is the permittivity at constant stress. If we consider a thin piezoelectric patch, the stress and the electric field can be seen as constant along the thickness h_p [4]. Then, the normal force N_p is obtained by multiplying the stress by the patch cross-section area $S_p = bh_p$. Moreover, $E_p = -V_p/h_p$, where V_p is the voltage between the two electrodes. At the end, the electric charge Q_p comes from the integration of $-D_p$ all over the surface of the patch. It is thus found from Eq. (1) that

$$(2) \qquad \begin{cases} N_p = Y_p^E S_p \varepsilon_p - e_p V_p \\ Q_p = e_p \Delta U_p + C_p^{\varepsilon} V_p, \end{cases} \quad \text{where} \quad e_p = -b e_{31}, \quad C_p^{\varepsilon} = \frac{A_p \bar{\epsilon}_{33}^{\varepsilon}}{h_p} \quad \text{and} \quad A_p = b l_p.$$

The difference between the right and left end displacements of the patch, $\Delta U_p = U_{p\mathrm{R}} - U_{p\mathrm{L}}$, appears in the electrical equation together with C_p^{ε}, the capacitance obtained when no strain is allowed along the direction '1'.

However, Eq. (2) is valid only if the considered piezoelectric patch is free in its transverse directions. This is not true when the patch is bound to a main structure as it cannot freely extend in the

direction '2'. This effect was analyzed by Maurini et al. [5] who presented corrected 1D coefficients obtained from a 3D formulation. For example, even if no external force is applied, the patch is constrained by the elastic material on which it is glued. Consequently, its capacitance is significantly lower than the free capacitance of a free single patch. For $h_p/h_s \ll 1$ and relatively close Poisson ratios in the patch and in the the main structure, the free capacitance can be approximated by

$$C_p^\sigma = \frac{A_p \epsilon_{33}^p}{h_p}\left(1 + 12k_{31}^2 \frac{1+\nu_p^E}{1-\nu_p^E-2k_{31}^2}\frac{Y_p^E}{Y_s}\frac{h_p}{h_s}\right), \quad \text{where} \quad \epsilon_{33}^p = \epsilon_{33}^\sigma\left(1 - \frac{2k_{31}^2}{1-\nu_p^E}\right) \tag{3}$$

and $k_{31}^2 = d_{31}^2/(s_{11}^E \epsilon_{33}^\sigma)$. It is seen that the result depends on Y_s, the Young modulus of the main structure, and ν_p^E, the Poisson ratio of the patch at constant electric field.

3. Transfer matrix models for longitudinal wave propagation

3.1 Discrete model based on global properties

The unit cell illustrated in Fig. 1 presents a composite laminate made of an elastic rod portion symmetrically covered with two piezoelectric patches. This structure can be firstly seen as an homogenized medium governed by a global piezoelectric coupling of the form of Eq. (2). Then, if the considered wavelength is large compared to the length a of the unit cell, the strain can be approximated by $\varepsilon \approx \Delta U/a$, where $\Delta U = U_\mathrm{R} - U_\mathrm{L}$ is the difference between the right and left displacements at the ends of the unit cell. Consequently, the normal force N depends on a global stiffness K_E and this leads to the following discrete model:

$$\begin{cases} N = K^E \Delta U - eV_I \\ Q_I = e\Delta U + C^\varepsilon V_I, \end{cases} \quad \text{where} \quad \frac{1}{K^E} = \frac{l_p}{Y_s S_s + 2Y_p^E S_p} + \frac{a-l_p}{Y_s S_s} \quad \text{and} \quad S_s = bh_s. \tag{4}$$

Even if K^E can be easily obtained, the determination of the global coupling e and the global blocked capacitance C^ε requires further analysis. C^ε is the capacitance obtained when $\Delta U = 0$. It differs from C^σ, the global capacitance obtained when $N = 0$. This one can be determined from the knowledge of the free capacitance C_p^σ. Furthermore, K^D, the stiffness in open circuit ($Q_I = 0$), is calculated in the same way as K^E by replacing Y_p^E by Y_p^D in Eq. (4). The Young modulus at constant electric displacement, Y_p^D, is related to the other material constants as it is found from Eq. (1) that $Y_p^D = Y_p^E + \bar{e}_{31}^2/\bar{\epsilon}_{33}^\varepsilon$. Finally, Eq. (1) gives the expressions for the remaining global constants:

$$\begin{cases} e = \sqrt{K^E\left(1 - \dfrac{K^E}{K^D}\right)C^\sigma} \\ C^\varepsilon = C^\sigma \dfrac{K^E}{K^D} \end{cases} \quad \text{where} \quad C^\sigma = 2C_p^\sigma \quad \text{and} \quad \frac{1}{K^D} = \frac{l_p}{Y_s S_s + 2Y_p^D S_p} + \frac{a-l_p}{Y_s S_s}. \tag{5}$$

From a mechanical point of view, the discrete model can be illustrated by Fig. 2(a), where the total mass of the unit cell is discretized in two half masses $m/2 = (\rho_s S_s a + 2\rho_p S_p l_p)/2$, where ρ_s and ρ_p are the densities of the rod and the patches. By taking into account the electrical network that is connected to the patches as it is illustrated in Fig. 1, the discrete electromechanical unit cell can be represented by the electric scheme seen in Fig. 3. The unit cell can then be described by a transfer matrix formulation relating the electromechanical state vectors at its right and left ends [3]:

$$\begin{bmatrix} U_\mathrm{R} \\ Q_\mathrm{R} \\ N_\mathrm{R} \\ V_\mathrm{R} \end{bmatrix} = \begin{bmatrix} 1-f & \dfrac{e}{K^E C^\varepsilon}\hat{f} & \dfrac{1}{K^E} & \dfrac{e}{K^E} \\ ef & 1-\Lambda\hat{f} & -\dfrac{e}{K^E} & -\Lambda C^\varepsilon \\ -2K^E f\left(1-\dfrac{f}{2}\right) & -\dfrac{e}{C^\varepsilon} f\hat{f} & 1-f & -ef \\ \dfrac{e}{C^\varepsilon} f\hat{f} & \dfrac{2}{C^\varepsilon}\hat{f}\left(1-\dfrac{\Lambda\hat{f}}{2}\right) & -\dfrac{e}{K^E C^\varepsilon}\hat{f} & 1-\Lambda\hat{f} \end{bmatrix} \begin{bmatrix} U_\mathrm{L} \\ Q_\mathrm{L} \\ N_\mathrm{L} \\ V_\mathrm{L} \end{bmatrix}, \tag{6}$$

where $f = \omega^2 m/(2K^E)$, $\hat{f} = \omega^2 LC^\varepsilon/2$ and $\Lambda = 1 + e^2/(K^E C^\varepsilon)$.

3.2 Full homogenized mechanical model

If it is decided to keep the continuity of the mechanical medium, the unit cell can no more be described by a lattice of point masses but requires an homogenized rod model as presented in Fig. 2(b). The Young modulus Y^E, the density ρ and the cross-section area S come from an homogenization along the whole unit cell. Ones obtains an homogenized model, where the definition of e and C^ε remains the same as in the discrete model:

$$\text{(7)} \qquad \begin{cases} N = Y^E S\varepsilon - eV_I \\ Q_I = e\Delta U + C^\varepsilon V_I, \end{cases} \quad \text{where} \quad Y^E = \frac{K^E a}{S} \quad \text{and} \quad S = S_s + 2S_p\frac{l_p}{a}.$$

It can be seen from Fig. 2(b) that a force $N_\text{R} + eV_I$ is applied on the right of a rod portion and a force $-(N_\text{L} + eV_I)$ is applied on its left. Consequently, a classical rod transfer matrix [1] can be used to described the relation between those two forces and the corresponding end displacements:

$$\text{(8)} \qquad \begin{bmatrix} U_\text{R} \\ N_\text{R} + eV_I \end{bmatrix} = \boldsymbol{T_m} \begin{bmatrix} U_\text{L} \\ N_\text{L} + eV_I \end{bmatrix}, \quad \text{where} \quad \boldsymbol{T_m} = \begin{bmatrix} \cos(ka) & \dfrac{\sin(ka)}{Y^E Sk} \\ -Y^E Sk\sin(ka) & \cos(ka) \end{bmatrix},$$

The wave number k is obtained from the rod dispersion relation $k = \omega\sqrt{\rho/Y^E}$, where $\rho = m/(Sa)$ is the homogenized density of the unit cell. The voltage V_I still appears in Eq. (8) but as the electrical part of the problem are unchanged, it can be determined from Fig. 3 that

$$\text{(9)} \qquad V_I = [\frac{L}{2}\omega^2 \;\; 1] \begin{bmatrix} Q_\text{L} \\ V_\text{L} \end{bmatrix} = [-\frac{L}{2}\omega^2 \;\; 1] \begin{bmatrix} Q_\text{R} \\ V_\text{R} \end{bmatrix}$$

Moreover, the relation between the electrical state vectors is also obtained from Fig. 3:

$$\text{(10)} \qquad \begin{bmatrix} Q_\text{R} \\ V_\text{R} \end{bmatrix} = \boldsymbol{T_e} \begin{bmatrix} Q_\text{L} \\ V_\text{L} \end{bmatrix} - e\Delta U \begin{bmatrix} 1 \\ \dfrac{L}{2}\omega^2 \end{bmatrix} \quad \text{where} \quad \boldsymbol{T_e} = \begin{bmatrix} 1-\hat{f} & -C^\varepsilon \\ \dfrac{2}{C^\varepsilon}\hat{f}(1-\dfrac{\hat{f}}{2}) & 1-\hat{f} \end{bmatrix}$$

Combining Eqs. (8), (9) and (10) leads to the following matrix system that enables the determination of the transfer matrix for the homogenized model:

$$\text{(11)} \qquad \begin{bmatrix} \boldsymbol{I_2} & \boldsymbol{0} \\ e\begin{bmatrix} 1 & 0 \\ \frac{L}{2}\omega^2 & 0 \end{bmatrix} & \boldsymbol{I_2} \end{bmatrix} \begin{bmatrix} \boldsymbol{I_2} & e\begin{bmatrix} 0 & 0 \\ -\frac{L}{2}\omega^2 & 1 \end{bmatrix} \\ \boldsymbol{0} & \boldsymbol{I_2} \end{bmatrix} \begin{bmatrix} U_R \\ N_R \\ Q_R \\ V_R \end{bmatrix} = \begin{bmatrix} \boldsymbol{T_m} & e\boldsymbol{T_m}\begin{bmatrix} 0 & 0 \\ \frac{L}{2}\omega^2 & 1 \end{bmatrix} \\ e\begin{bmatrix} 1 & 0 \\ \frac{L}{2}\omega^2 & 0 \end{bmatrix} & \boldsymbol{T_e} \end{bmatrix} \begin{bmatrix} U_L \\ N_L \\ Q_L \\ V_L \end{bmatrix},$$

At last, it is remarked that the resulting transfer matrix is equal to the one presented in Eq. (6) after applying the operation that transforms a lattice into a continuous rod [3], i.e.

$$\text{(12)} \qquad f \to 1 - \cos(ka) \quad \text{and} \quad K^E \to \frac{Y^E S}{a}\frac{ka}{\sin(ka)}.$$

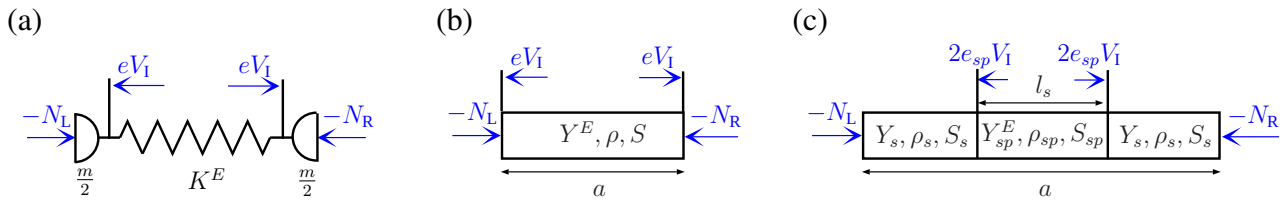

Figure 2: Three models for the unit cell: (a) Discrete model. (b) Full homogenized model. (c) Piecewise homogenized model.

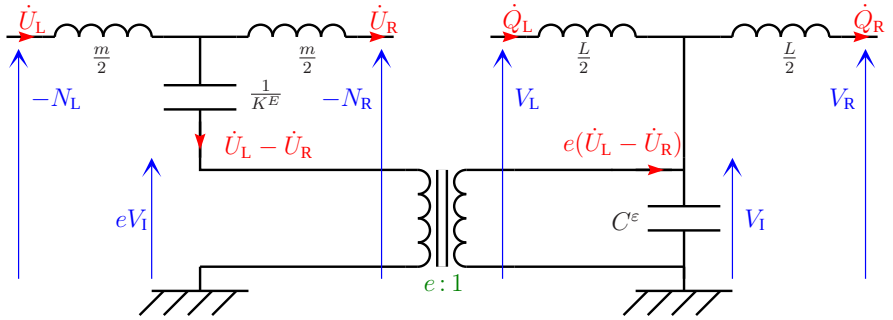

Figure 3: Discrete model of the electromechanical unit cell.

3.3 Piecewise homogenized mechanical model

A piecewise homogenized one-dimensional model of the unit cell requires to take into account the mechanical discontinuity created by the addition of patches on the main structure. This can be illustrated by the model presented in Fig. 2(c), where three different rod portions are connected together. The central portion 'sp' represent the part of the structure which is covered by the patches. By considering a normal force N_{sp} in this rod portion, the problem can be expressed under the same form as Eqs. (2) and (4):

$$(13) \qquad \begin{cases} N_{sp} = Y_{sp}^E S_{sp} \varepsilon_{sp} - e_{sp} V_I \\ Q_I = e_{sp} \Delta U_{sp} + C_{sp}^\varepsilon V_I, \end{cases} \quad \text{where} \quad Y_{sp}^E = \frac{Y_s S_s + 2 Y_p^E S_p}{S_{sp}} \quad \text{and} \quad S_{sp} = S_s + 2S_p.$$

The constants referring to the 'sp' portion differ from the ones obtained for the discrete model as the two patches don't cover the entire cell length ($a \neq l_p$). Nevertheless, e_{sp} and C_{sp}^ε are determined with the same method as in Eq. (5). The system of equations (13) can be transform in a transfer matrix formulation by remarking that the problem focusing on the 'sp' rod portion is equivalent to the one presented for the homogenized model with $\rho_{sp} = (\rho_s S_s + 2\rho_p S_p)/S_{sp}$, which is the homogenized density of the 'sp' rod portion. As the two 's' rod portions are purely elastic, their mechanical transfer matrices $\boldsymbol{T_s}$ can be determined in the same way as $\boldsymbol{T_m}$ but with the use of the constants Y_s, ρ_s and S_s. Finally, if the 4×4 matrix $\boldsymbol{T_{sp}}$ describe the 'sp' rod portion, the problem can be expressed as

$$(14) \qquad \begin{bmatrix} U_R \\ N_R \\ Q_R \\ V_R \end{bmatrix} = \begin{bmatrix} \boldsymbol{T_s} & \boldsymbol{0} \\ \boldsymbol{0} & \boldsymbol{I_2} \end{bmatrix} \boldsymbol{T_{sp}} \begin{bmatrix} \boldsymbol{T_s} & \boldsymbol{0} \\ \boldsymbol{0} & \boldsymbol{I_2} \end{bmatrix} \begin{bmatrix} U_L \\ N_L \\ Q_L \\ V_L \end{bmatrix}, \quad \text{where} \quad \boldsymbol{I_2} = \begin{bmatrix} 1 & 0 \\ 0 & 1 \end{bmatrix}.$$

3.4 Finite element model

The three previous models are based on analytic formulations but the electromechanical transfer matrix can also be obtained from a finite element analysis. The considered numerical model is the one presented by Thomas et al. [4] for the analysis of shunted thin piezoelectric patches. In the present case involving two patches connected in parallel, the finite element formulation can be simplified in the following form:

$$(15) \qquad \begin{bmatrix} \boldsymbol{M_m} & \boldsymbol{0} \\ \boldsymbol{0} & 0 \end{bmatrix} \begin{bmatrix} \ddot{\boldsymbol{U}} \\ \ddot{V}_I \end{bmatrix} + \begin{bmatrix} \boldsymbol{K_m} & \boldsymbol{K_c} \\ -\boldsymbol{K_c}^{\boldsymbol{T}} & C_{sp}^\varepsilon \end{bmatrix} \begin{bmatrix} \boldsymbol{U} \\ V_I \end{bmatrix} = \begin{bmatrix} \boldsymbol{N} \\ Q_I \end{bmatrix} \quad \text{where} \quad \boldsymbol{U} = \begin{bmatrix} U_L \\ \boldsymbol{U_I} \\ U_R \end{bmatrix} \quad \text{and} \quad \boldsymbol{N} = \begin{bmatrix} -N_L \\ \boldsymbol{0} \\ N_R \end{bmatrix}.$$

$\boldsymbol{M_m}$, $\boldsymbol{K_m}$ and $\boldsymbol{K_c}$ are respectively the mass, stiffness and coupling matrices that are defined in [4], with a restriction to the longitudinal case for the present example. As the patches are not shunted by an impedance but connected to a network, the electrical components cannot be condensed in the mechanical problem. Nevertheless, it is still possible to define the electric charge Q_I relatively to a charge

vector $\boldsymbol{Q} = \left[\begin{array}{cc} Q_L & Q_R \end{array}\right]^T$, as well as the relation between a voltage vector $\boldsymbol{V} = \left[\begin{array}{cc} -V_L & V_R \end{array}\right]^T$ and the voltage V_I:

$$Q_I = \boldsymbol{S_Q Q} \quad \text{and} \quad \boldsymbol{V^Q} = \boldsymbol{S_V} V_I{}^{\boldsymbol{Q}} = \boldsymbol{S_V} V_I{}^{Q_I} = \frac{1}{C_{sp}^{\varepsilon}} \boldsymbol{S_V K_c{}^T U}. \tag{16}$$

For the voltage, only the relation with no displacement of the electric charges is required ($\boldsymbol{Q} = \boldsymbol{0} \Rightarrow Q_I = 0$). Equation (16) thus depends on the topology of the electrical network and the one presented in Fig. 3 gives $\boldsymbol{S_Q} = \left[\begin{array}{cc} 1 & -1 \end{array}\right]$ and $\boldsymbol{S_V} = \left[\begin{array}{cc} -1 & 1 \end{array}\right]^T$. At the end, Eqs. (15) and (16) enable to find the following matrix formulation:

$$\left[\left[\begin{array}{cc} \boldsymbol{K_m} + \frac{1}{C_{sp}^{\varepsilon}} \boldsymbol{K_c K_c{}^T} & \frac{1}{C_{sp}^{\varepsilon}} \boldsymbol{K_c S_Q} \\ \frac{1}{C_{sp}^{\varepsilon}} \boldsymbol{S_V K_c{}^T} & \boldsymbol{K_e} \end{array}\right] - \omega^2 \left[\begin{array}{cc} \boldsymbol{M_m} & \boldsymbol{0} \\ \boldsymbol{0} & \boldsymbol{M_e} \end{array}\right]\right] \left[\begin{array}{c} \boldsymbol{U} \\ \boldsymbol{Q} \end{array}\right] = \left[\begin{array}{c} \boldsymbol{N} \\ \boldsymbol{V} \end{array}\right], \tag{17}$$

where $\boldsymbol{K_e} = -\left[\begin{array}{cc} \frac{1}{C_{sp}^{\varepsilon}} & -\frac{1}{C_{sp}^{\varepsilon}} \\ -\frac{1}{C_{sp}^{\varepsilon}} & \frac{1}{C_{sp}^{\varepsilon}} \end{array}\right]$ and $\boldsymbol{M_e} = -\left[\begin{array}{cc} \frac{L}{2} & 0 \\ 0 & \frac{L}{2} \end{array}\right]$ are analogues of mass and stiffness matrices, which still refer to the electrical network described in Fig. 3. The dynamic stiffness matrix presented in Eq. (17) is then rearranged to bring together the mechanical and electrical components on the left and on the right of the unit cell:

$$\left[\begin{array}{ccc} \boldsymbol{\tilde{D}_{LL}} & \boldsymbol{\tilde{D}_{LI}} & \boldsymbol{\tilde{D}_{LR}} \\ \boldsymbol{\tilde{D}_{IL}} & \boldsymbol{\tilde{D}_{II}} & \boldsymbol{\tilde{D}_{IR}} \\ \boldsymbol{\tilde{D}_{RL}} & \boldsymbol{\tilde{D}_{RI}} & \boldsymbol{\tilde{D}_{RR}} \end{array}\right] \left[\begin{array}{c} \boldsymbol{q_L} \\ \boldsymbol{q_I} \\ \boldsymbol{q_R} \end{array}\right] = \left[\begin{array}{c} \boldsymbol{-F_L} \\ \boldsymbol{0} \\ \boldsymbol{F_R} \end{array}\right] \quad \text{where} \quad \boldsymbol{F_L} = \left[\begin{array}{c} \boldsymbol{N_L} \\ \boldsymbol{V_L} \end{array}\right], \quad \boldsymbol{F_R} = \left[\begin{array}{c} \boldsymbol{N_R} \\ \boldsymbol{V_R} \end{array}\right], \tag{18}$$

$\boldsymbol{q_L} = \left[\begin{array}{cc} U_L & Q_L \end{array}\right]^T$, $\boldsymbol{q_I} = \boldsymbol{U_I}$ and $\boldsymbol{q_R} = \left[\begin{array}{cc} U_R & Q_R \end{array}\right]^T$. With this partitioning, the procedures of the waveguide finite element methods [6] can be implemented. It starts with an elimination of the interior degrees of freedoms

$$\left[\begin{array}{cc} \boldsymbol{D_{LL}} & \boldsymbol{D_{LR}} \\ \boldsymbol{D_{RL}} & \boldsymbol{D_{RR}} \end{array}\right] \left[\begin{array}{c} \boldsymbol{q_L} \\ \boldsymbol{q_R} \end{array}\right] = \left[\begin{array}{c} \boldsymbol{-F_L} \\ \boldsymbol{F_R} \end{array}\right], \quad \text{where} \quad \left\{\begin{array}{l} \boldsymbol{D_{LL}} = \boldsymbol{\tilde{D}_{LL}} - \boldsymbol{\tilde{D}_{LI}} \boldsymbol{\tilde{D}_{II}^{-1}} \boldsymbol{\tilde{D}_{IL}} \\ \boldsymbol{D_{LR}} = \boldsymbol{\tilde{D}_{LR}} - \boldsymbol{\tilde{D}_{LI}} \boldsymbol{\tilde{D}_{II}^{-1}} \boldsymbol{\tilde{D}_{IR}} \\ \boldsymbol{D_{RL}} = \boldsymbol{\tilde{D}_{RL}} - \boldsymbol{\tilde{D}_{RI}} \boldsymbol{\tilde{D}_{II}^{-1}} \boldsymbol{\tilde{D}_{IL}} \\ \boldsymbol{D_{RR}} = \boldsymbol{\tilde{D}_{RR}} - \boldsymbol{\tilde{D}_{RI}} \boldsymbol{\tilde{D}_{II}^{-1}} \boldsymbol{\tilde{D}_{IR}} \end{array}\right., \tag{19}$$

followed by a transformation of the condensed dynamic stiffness matrix into a transfer matrix:

$$\left[\begin{array}{c} U_R \\ Q_R \\ N_R \\ V_R \end{array}\right] = \left[\begin{array}{cc} \boldsymbol{-D_{LR}^{-1} D_{LL}} & \boldsymbol{D_{LR}^{-1}} \\ \boldsymbol{-D_{RL} + D_{RR} D_{LR}^{-1} D_{LL}} & \boldsymbol{-D_{RR} D_{LR}^{-1}} \end{array}\right] \left[\begin{array}{c} U_L \\ Q_L \\ N_L \\ V_L \end{array}\right]. \tag{20}$$

4. Comparison of the transfer matrix models

4.1 Finite periodic structure

The previous models are compared by considering the example of a free-free rod covered with $n = 20$ pairs of piezoelectric patches. Table 1 gives the geometry and the material properties of the unit cell illustrated in Fig. 1. The twenty successive unit cells are electrically connected with a line of inductors having an identical value $L = m/(K^E C^{\varepsilon})$. When short circuiting the two ends of the

Table 1: Geometry and material properties.

	Rod (Aluminum 2017)	Patches (PZT)
Length (mm)	$l_s = na = 200 \times 50$	$l_p = 30$
Width (mm)	$b = 20$	$b = 20$
Thickness (mm)	$h_s = 20$	$h_p = 5$
Density kg/m^3	$\rho_s = 2780$	$\rho_p = 7800$
Young modulus (GPa)	$Y_s = 73.9$	$1/s_{11}^E = 66.7$
Charge constant (pC/N)	-	$d_{31} = -210$
Permittivity (nF/m)	-	$\epsilon_{33}^\sigma = 21.2$

network, this modal coupling condition tunes the electrical modes to the ones of the mechanical lattice used in the discrete model [3]. A tuned mass effect can thus be obtained on several modes together and the vibration amplitudes are reduced by introducing damping in the network. In the present example, a resistance $R_s = 3\,\Omega$ is serially added to the inductors by replacing L by $L - jR_s/\omega$, where $j^2 = -1$.

For a finite structure consisting of n identical unit cells, the most classical way to obtain the relation between the states at both ends of the structure requires raising the corresponding transfer matrix to the power of n.

4.2 Comparison of the frequency response functions

The models are firstly compared in a frequency range, where appear the first longitudinal modes the rod. The frequency response functions obtained with the discrete and the piecewise homogenized one-dimensional model are represented in Fig 4. The results coming from the homogenized and the finite element model are not explicitly represented, as their difference with the piecewise homogenized model are not observable on this frequency range. It can be remarked that the discrete model is no more reliable when the wavelength approaches the length of the unit cell. The position of the mechanical resonances are shifted because the mechanical medium is modeled by a lattice. Then, when the network is tuned to this lattice, the discrete model doesn't take into account the increasing mistuning between the continuous and the discrete structure.

The second comparison is made at higher frequencies, when the considered wavelength is close to the length of the unit cells. It is still verified that the finite element model tends to the piecewise homogenized model, but the homogenized model now presents a significantly different response, as seen in Fig 5. Actually, the piecewise homogenized model presents a stop band phenomenon around 50 kHz due to the mechanical discontinuity in the unit cell. This stop band is clearly observable in the analysis of the propagation constant of the corresponding transfer matrix. At the same time, it does not appear with the homogenized model as the mechanical discontinuity induced by the addition of

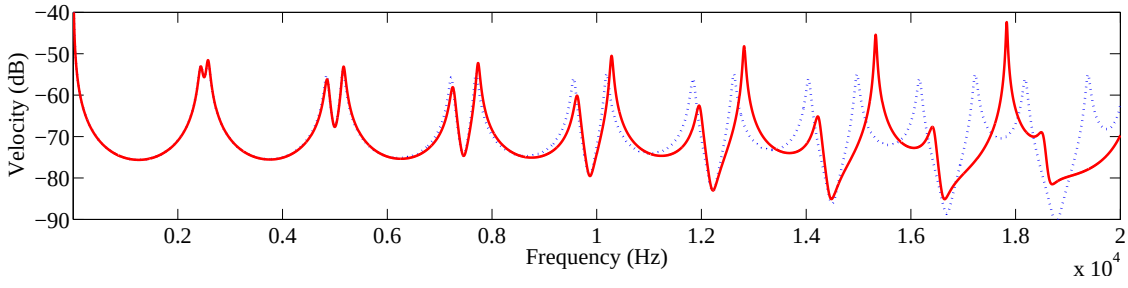

Figure 4: Response functions at low frequencies - (· · ·) for the discrete model, (—) for the piecewise homogenized model.

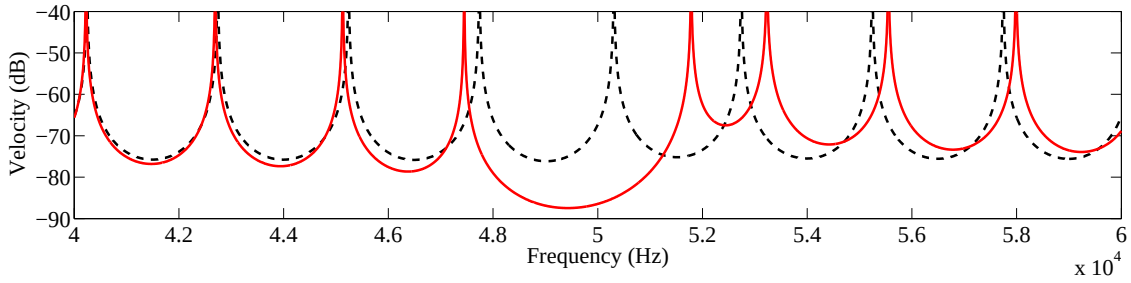

Figure 5: Response functions at higher frequencies - (− −) for the homogenized model, (—) for the piecewise homogenized model.

the patches is not taken into account. Yet, it can still be observed that the considered frequency range is clearly beyond the last electrical resonances. The control strategy has thus almost no effect here, which question the interest of an analysis at such high frequencies.

5. Conclusions

In this paper, four electromechanical transfer matrix models have been presented and compared for passive vibration damping using an array of piezoelectric patches. While the electrical medium is discrete, the mechanical structure can be approximated either by its discrete equivalent, by a piecewise or full homogenized model, or by a finite element model. The main advantage of the discrete model is its simplicity. It is useful to understand the multimodal coupling, but it is limited to a maximal frequency related to the number of unit cells per wavelength (here 10 unit cell per wavelength to damp the first four modes of the rod). The full homogenized model allows taking into account the mechanical continuity. It can be easily derived from the discrete transfer matrix and is sufficiently accurate on the frequency range where the multimodal control is sought. The piecewise homogenized model is adapted to analyze the stop-band induced by the mechanical discontinuities. However, this phenomenon, which occurs for wavelength equal to the length of the unit cell, is outside the scope of the multimodal control since the electrical resonances are placed at lower frequencies. Finally, the finite element model tends to the piecewise homogenized model when increasing the number of elements. Future works will be dedicated to the application of the proposed approach to bending motions.

REFERENCES

1. Thorp, O., Ruzzene, M., and Baz, A. Attenuation and localization of wave propagation in rods with periodic shunted piezoelectric patches, *Smart Materials and Structures*, **10** (5), 979 (2001).

2. Maurini, C., Dell'Isola, F., and Del Vescovo, D. Comparison of piezoelectronic networks acting as distributed vibration absorbers, *Mechanical Systems and Signal Processing*, **18** (5), 1243–1271 (2004).

3. Lossouarn, B., Aucejo, M., and Deü, J. F. Multimodal coupling of periodic lattices and application to rod vibration damping with a piezoelectric network, *Smart Materials and Structures*, **24** (4), 045018, (2015)

4. Thomas, O., Deü, J. F., and Ducarne, J. Vibrations of an elastic structure with shunted piezoelectric patches: efficient finite element formulation and electromechanical coupling coefficients, *International Journal for Numerical Methods in Engineering*, **80** (2), 235–268, (2009).

5. Maurini, C., Pouget, J., and Dell'Isola, F. Extension of the Euler-Bernoulli model of piezoelectric laminates to include 3D effects via a mixed approach, *Computers and Structures*, **84** (22), 1438–1458, (2006).

6. Mace, B. R., Duhamel, D., Brennan, M. J., and Hinke, L. Finite element prediction of wave motion in structural waveguides, *The Journal of the Acoustical Society of America*, **117** (5), 2835–2843 (2005).